Molecular dynamics-based simulations to study crack tip interaction with symmetrical and asymmetrical tilt grain boundaries in zirconium

Article *in* Journal of Nuclear Materials · July 2019

DOI: 10.1016/j.jnucmat.2019.151739

CITATION
1

READS
45

5 authors, including:

Avinash Parashar
Indian Institute of Technology Roorkee
84 PUBLICATIONS **478** CITATIONS
SEE PROFILE

Divya Singh
Johns Hopkins University
13 PUBLICATIONS **31** CITATIONS
SEE PROFILE

Kedharnath Arumugakani
Bhabha Atomic Research Centre
5 PUBLICATIONS **16** CITATIONS
SEE PROFILE

Apu Sarkar
Bhabha Atomic Research Centre
137 PUBLICATIONS **1,182** CITATIONS
SEE PROFILE

Journal of Nuclear Materials 526 (2019) 151739

Contents lists available at ScienceDirect

Journal of Nuclear Materials

journal homepage: www.elsevier.com/locate/jnucmat

Molecular dynamics-based simulations to study crack tip interaction with symmetrical and asymmetrical tilt grain boundaries in Zr

Divya Singh [a], Avinash Parashar [a, *], A. Kedharnath [b], Rajeev Kapoor [b], Apu Sarkar [b]

[a] Department of Mechanical and Industrial Engineering, Indian Institute of Technology, Roorkee, India
[b] Mechanical Metallurgy Division, Bhabha Atomic Research Center, Mumbai, 400085, India

ARTICLE INFO

Article history:
Received 5 March 2019
Received in revised form
19 June 2019
Accepted 31 July 2019
Available online 1 August 2019

Keywords:
Bi-crystals
Crack tip
Fracture properties
Disclination shielding
Irradiation
hcp-Zr

ABSTRACT

In this article, molecular dynamics based simulations were carried out to study the fracture behaviour of bi-crystalline zirconium (Zr). Atomistic simulations were performed to study the effect of grain boundary configuration on the crack tip behaviour subjected to opening mode of loading. Separate set of simulations were carried out to study the influence of crack orientation on the failure morphology, and strength of bi-crystalline Zr. Disclination shielding of the crack tip stresses induced by grain boundaries, significantly affects the fracture behaviour of bi-crystalline Zr. Opening stresses at the crack tip varied as a function of distance between crack tip and grain boundary plane. Crack propagation and blunting of tip was also predicted as the function of distance from the grain boundary plane. Effect of irradiation induced point defects have also been studied with respect to spatial distribution and number of defects.

1. Introduction

Due to superior mechanical properties and low neutron absorption cross section, Zirconium (Zr) is the most widely used nuclear material. Though, nuclear power plants are in use for many decades, but still the literature is almost mute on the mechanical and fracture properties of nuclear materials such as Zr and Zr-Nb alloys. Designing of nuclear structures requires selection of material that can withstand extreme and complex loading scenario.

Grain boundaries play a significant role in improving the strength as well as fracture toughness of polycrystalline materials. According to Hall-Petch relationship, grain boundaries helps in enhancing the strength of poly-crystalline materials [1,2]. However, a decrease in grain size below one micrometre leads to softening, instead of hardening, due to phenomenon such as grain boundary migration and sliding [3–11]. Hodge et al. [12] have reported improvement in the fracture toughness of coarse grain material on grain refinement. Similar kind of experimental observations were also reported by Tsuji et al. [13] and Tanaka et al. [14]. Noronha and Farkas [15] have employed atomistic simulations in conjunction with dislocation dynamics to investigate the effect of grain boundaries on the fracture toughness of α-iron and aluminium. Zeng and Hartmaeir [16] have studied the effect of crystal size on the fracture toughness of polycrystalline tungsten. Shimokawa et al. [17] employed molecular dynamics based atomistic simulations to study the interaction between crack tip, dislocations and grain boundaries in bi-crystals of aluminium. They have elucidated the role of grain boundaries not only as obstacles, but also as a source of dislocations.

Griffith and his research team employed X-ray diffraction line broadening analysis based technique to study the distribution of dislocations in highly textured Zr-2.5Nb alloy. It was concluded in their experimental work that dislocation densities in Zr-2.5Nb alloys are highly dependent on the inter-granular strains [18]. Bailey [19] employed tunnelling electron microscopy to study the distribution of dislocations in Zr. It was observed in his experiments that distribution of dislocations depends on the content of oxygen and nitrogen in Zr. At a lower percentage content of oxygen and nitrogen (0.03%) the dislocations were observed as tangles or in loops, whereas at a higher content (0.1%) dislocations were comparatively straight and restricted to {0–110} planes. Rafique [20] et al. carried out experiments to elucidate the tensile behaviour of irradiated polycrystalline Zr. It was reported in their work that irradiation has negligible effect on the mechanical properties

* Corresponding author.
E-mail address: drap1fme@iitr.ac.in (A. Parashar).

https://doi.org/10.1016/j.jnucmat.2019.151739
0022-3115/

of Zr. Shah and his team of researchers have experimentally evaluated the fracture toughness of pressure tube made up of Zr-2.5Nb alloy [21]. They reported a value of lower fracture toughness at room temperature that starts improving with the increase in temperature, and finally become saturated at a temperature of 250 °C [21]. Kapoor et al. [22] employed the concepts of elastic-plastic fracture mechanics to study the effect of certain trace elements on the fracture toughness of Zr-2.5Nb pressure tubes. Himbeault et al. [23] have also studied the fracture toughness of irradiated Zr-2.5Nb pressure tube material in the range of room temperature to 300 °C. Their study was focused on developing a mechanism for reduction in the fracture toughness of Zr-2.5Nb tube materials with the increase in neutron irradiation damage.

So far, literature is almost mute on the effect of grain boundaries and irradiation induced defects on the fracture behaviour of nuclear materials like Zr, Nb and Zr-Nb alloys [29–35]. In this article, efforts have been made by the authors to study the effect of grain boundary stresses on the crack tip behaviour in a bi-crystal of Zr. In order to keep the atomistic model, close to realistic one, symmetrical and asymmetrical tilt grain boundaries were generated along [0001] as the tilt axes, which resembles the structure reported in the experimental work [36]. In addition to the effect of grain boundaries, simulations have also been performed to study the effect of irradiation-induced point defects on the fracture behaviour of bi-crystalline Zr. Several studies have been reported on the broad aspect of fracture behaviour of irradiated nuclear components, but they are limited in revealing the physics behind the crack tip behaviour in such complex and extreme environment conditions.

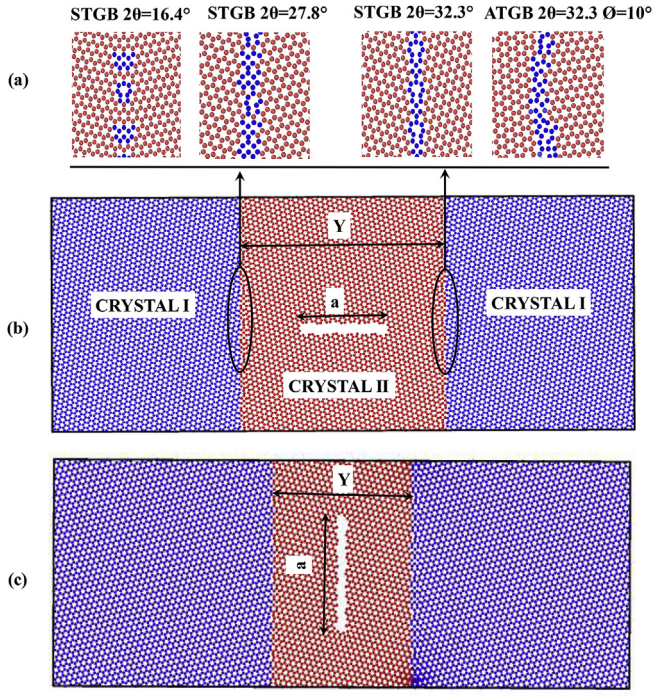

Fig. 1. Schematic of the simulation box for bi-crystal Zr (a) STGB and ATGB configurations at different misorientation angles (b) Bi-crystalline Zr with crack perpendicular to the GB plane (type-I) (c) Bi-crystalline Zr with crack front parallel to GB plane (type-II) (Y is the distance between the GB planes and a is the crack length).

2. Simulation details

In this article, molecular dynamics based simulations were carried out in parallel Large Scale Atomic/Molecular Massively Parallel Simulator (LAMMPS) [25], and post processing of dump files was performed in OVITO [26]. Embedded atomic method (EAM) force field parameters proposed by Mendeleev and Auckland (potential#2) was used for capturing inter-atomic forces between the atoms of Zr [24]. This potential is considered as more appropriate for capturing the formation of stable vacancy clusters and vacancy type dislocation loops [28]. The same potential has also been used by the authors to capture the grain boundary energies between the bi-crystals of Zr, tilted along [0001] and [0–110] as axis [29].

All simulations were carried out in three stages. In stage one, three symmetric (STGB) and one asymmetric tilt grain boundaries (ATGB) were generated between crystal-I and crystal-II as illustrated in Fig. 1. Initial orientation of both the crystals were x $[1\bar{1}00]$ y $[11\bar{2}0]$ z [0001]. Crystal-I and crystal −II was rotated by an angle $+\theta$ and -θ, respectively to achieve a mis-orientation angle of 2θ. GB planes for each mis-orientation angle is provided in Table 1 along with $\sum$ coincidence site lattice (CSL) values. Symmetrical grain boundary structures were generated after rotating crystal I and II with equal tilt angle (tilt angle (**θ**) = ½*misorientation angle) in clockwise and anti-clock wise directions, respectively, whereas for asymmetrical tilt grain boundary structures, the structure obtained after STGB generation was further rotated together in one direction with an inclination angle as illustrated in Fig. 2.

These grain boundary structures were only formed along [0001] as the tilt axis. Periodic boundary conditions were imposed in all the three principal directions; and in order to avoid imperfections at the boundaries of simulation box, crystal-II was sandwiched between crystal-I as illustrated in Fig. 1 (b). The size of the simulation was decided by performing simulations iteratively to avoid any image interaction across the periodic boundaries in all three directions. Additionally, as the crack was generated in the x-y plane and grain boundaries were present on either side of the crack tip,

Table 1
Configuration details of three symmetric and one asymmetric tilt grain boundary tilted along [0001] axis for first and second set of crack. Also mentioned details of simulation box for different crack lengths.

S.No.	Misorientation angle (2θ)	Inclination angle (Ø)	Sigma value ($\sum$)	GB plane	Cell size (ÅxÅxÅ)	Number of atoms	Crack size (Å)	Y (Å)
				TYPE-I	**CRACK**			
1.	32.3	0	13	(13–40)	145 × 360 × 121	263534	90	120,150,210
2.	16.4	0	49	(35–80)	130 × 331 × 121	219052	90	120,150,210
3.	27.8	0	39	(25–70)	118 × 331 × 121	197662	90	120,150,210
4.	32.3	10			118 × 320 × 121	191613	90	120,150,210
				TYPE-II	**CRACK**			
1.	32.3	0			145 × 360 × 121	263534	60	50, 80,140
2.	16.4	0			130 × 331 × 121	219052	60	50, 80,140
3.	27.8	0			118 × 331 × 121	197662	60	50, 80,140
4.	32.3	10			118 × 320 × 121	191613	60	50,80,140

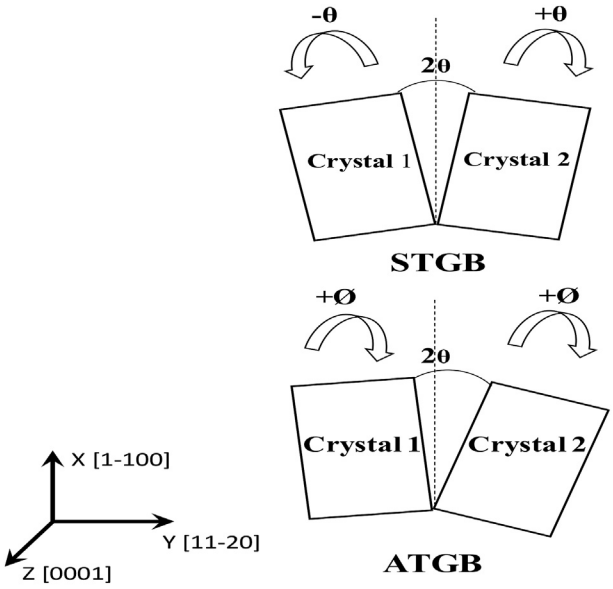

Fig. 2. Schematic of STGB and ATGB with the help of tilt (θ) and inclination angle(Ø).

periodic boundaries will not have an effect on the interaction of the crack tip with their periodic image. Simulations were carried out with different cell thickness and no strain hardening was observed on varying the simulation box size. Additionally, stacking sequence of the atoms (follow hcp crystal) was maintained and checked with the help of OVITO software. Multiple deletion criteria was applied in loop to get rid of overlapping atoms at GB in a range of 2.4 Å. Deletion criteria was applied in conjunction with conjugant gradient algorithm to obtain minimum energy configuration. In order to minimise the energy of the simulation box, tight force and energy tolerance values of 10^{-15} eV, 10^{-15} eV/Å, respectively selected for CG analysis. All the information required to generate STGB and ATGB are tabulated in Table 1. Grain boundary structures generated along [0001] as the tilt axis, more closely resembles the experimentally obtained GB configurations [36]. Due to six fold symmetry of hcp crystal along [0001] as the tilt axis, possible minimum and maximum mis-orientation angle ranges in between 0° and 60°. In order to cover the range of angles from lower mis-orientation to higher mis-orientation, three angles were considered, (a) 16.4° (b) 27.8° (c) 32.3°. It can be observed in Fig. 1 that at lower mis-orientation angle of 16.4°, dislocation cores separate out, whereas at higher mis-orientation angles dislocation cores merge into each other with higher density. Any further increase in mis-orientation angle above 32.3° will again separate out the dislocation cores and leads to lower mis-orientation angle.

After achieving minimum energy grain boundary configuration, crack was formed by removing two layers of atoms in crystal II, and the system was further relaxed under the influence of NPT ensemble for 45 ps with a time step of 0.001 ps to equilibrate the system at 1 K. In order to study the crack tip behaviour under the

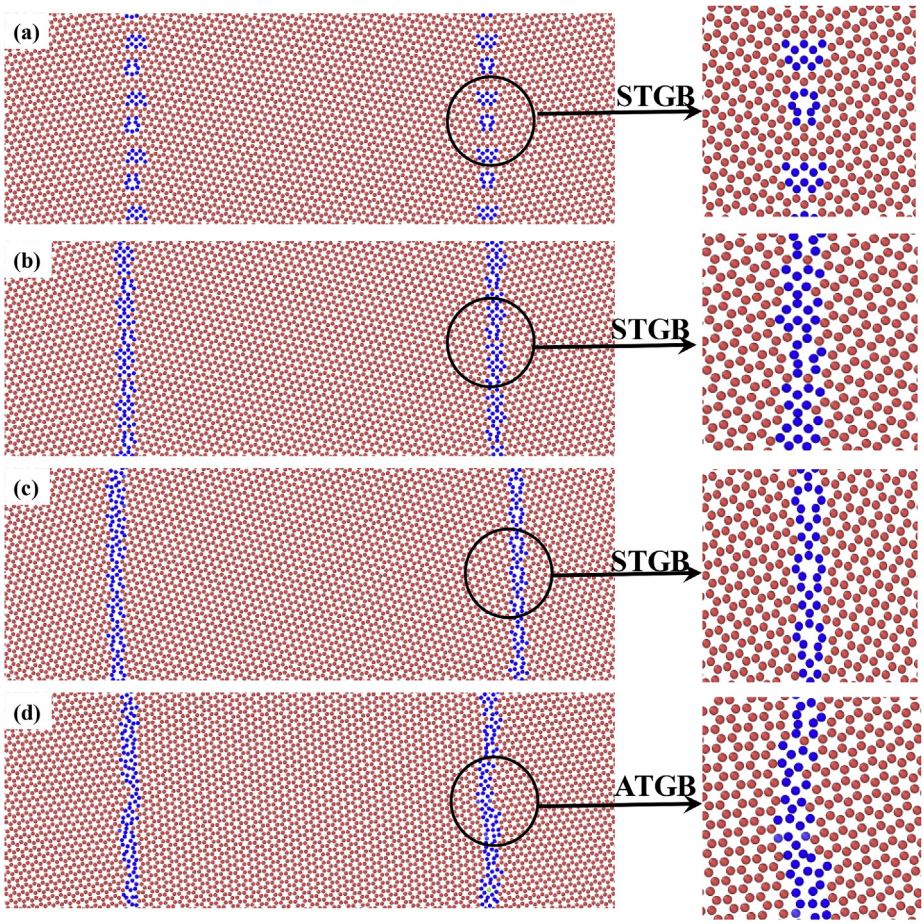

Fig. 3. GB structure for STGB with [0001]as the tilt axis with misorientation angles of (a) 16.4° (b) 27.8° (c) 32.3° (d) $2\theta = 32.3°$ and $Ø = 10°$. (Red atoms corresponds to hcp Zr, whereas blue coloured atoms are representing higher energy state atoms at the grain boundaries. Atoms are coloured by Common Neighbour Analysis (CNA) [42,43]). (For interpretation of the references to colour in this figure legend, the reader is referred to the Web version of this article.)

influence of grain boundary stresses, centrally embedded crack was generated in two different orientations. In first orientation, crack was kept perpendicular to the grain boundary plane as shown in Fig. 1(b), whereas in other orientation the crack was created parallel to the grain boundary plane (Fig. 1 c). Simulations were performed by varying the distance between the crack tip and grain boundary structures in the range of (15–60) Å, while keeping the crack length 'a' fixed. The distance between the grain boundary planes is marked as 'Y' in Fig. 1b and c. After finishing the equilibration, the simulation box was subjected to tensile deformation at a strain rate of 0.001/ps, along the direction perpendicular to the crack surfaces (mode I). Strain rate has significant effect on the mechanical properties of materials in atomistic simulations [38–41]. In order to perform this study, a constant strain rate value was employed in all the simulations, which helps in performing a comparative analysis of other parameters such as GB configuration, orientation of crack.

In the next stage of simulations, the effect of crack length (orientation perpendicular to grain boundaries) on the strength of bi-crystalline Zr was studied, while keeping the distance between the grain boundaries constant at 120 Å. In the third and final stage, simulations were performed to study the effect of irradiation induced defects on the crack tip behaviour. The simulations for generating point defects in the simulation box was performed under NVE ensemble at a temperature of 10 K. In order to perform these simulations, displacement cascades were run in the simulation box in front and at a varying distance from the crack tip. In order to generate irradiation induced defects, primary knock on atom (PKA) was selected in pre-defined positions in the simulation box. In order to ensure a stable number of point defects, the simulation box was divided in exterior and interior regions, where exterior region was used as a thermal bath, and maintained at a temperature of 10 K with the help of Noose Hover thermostat. The thickness of thermal bath in each principal direction was kept fixed at 20 Å. Selection of PKA was performed in such a manner that after assigning a value of kinetic energy equal to 2 keV the crack surfaces remain intact, without any damage from displacement cascade. From set of simulations performed with different spatial coordinate of PKA atoms, displacement cascade generated without damaging the crack surfaces were considered for further evaluation. Entire process of displacement cascade was simulated with three different set of integration time steps. Initially, integration time step of 10^{-4}ps was used for 30000 integration steps, which was raised to a value of 10^{-3}ps for another 30000 integration steps, and finally integration was performed at 0.002ps for another 30000 steps. These time steps were used to ensure formation of stable number of point defects in the simulation box. During the tensile deformation, the simulation box was always kept under the influence of NPT ensemble.

All the stresses referred in this article were estimated with the help of virial stress equation given below [37].

$$\sigma_{ij}^{a} = \frac{1}{\Omega}\left(\frac{1}{2}m^{a}v_{i}^{a}v_{j}^{a} + \sum r_{\alpha\beta}^{j} f_{\alpha\beta}^{i}\right) \quad (1)$$

where,

i,j = indices of Cartesian coordinate
Ω = atomic volume of atom a
α, β = atomic indices
m^a = mass of atom a
v^a = velocity of atom a
$r_{\alpha\beta}$ = distance between atoms α and β
$f_{\alpha\beta}^{i}$ = force on α atom due to β atom in direction i

3. Results and discussions

As stated in the previous section, simulations were carried out in three stages. In stage one, three symmetric and one asymmetric GB structures were generated in the simulation box, whereas second and third stage corresponds to the tensile deformation of bi-crystal of Zr, with or without point defects.

3.1. GB structures and energies

Atomic configurations of three symmetric and one asymmetrical tilt GB structures are shown in Fig. 3. It can be observed in Fig. 3a that in GB structures formed at lower tilt angle, dislocation cores were separated with a region of perfect crystal, whereas no such separation between dislocation cores were observed at higher values of misorientation angle as depicted in Fig. 3b and c. It is noteworthy that in case of STGBs, grain boundary structure is symmetric and ordered as shown in Fig. 3(a-c) as compared to disordered atomic configuration of ATGB shown in Fig. 3d. GB energies for STGB as well as ATGB configurations are tabulated in Table 2, and zero values of GB energy at misorientation angles of 0° and 60° corresponds to six-fold symmetry of STGB structures formed along [0001] as the tilt axis. At mis-orientation angles of

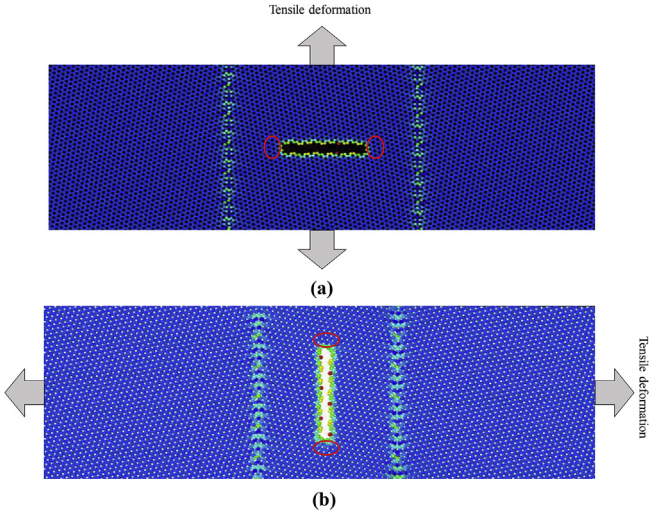

Fig. 4. Schematic of the bi-crystal with central crack (a) type I (b) type II direction of tensile loading with each crack orientations are marked with solid arrows.

Table 2
Grain boundary formation energies for STGB and ATGB configurations formed along [0001] as the tilt axis.

S.No.	Type of GB	Misorientation angle(2θ)	inclination angle(Ø)	GB energy (mJ/m^2)
1	STGB	0	0	0
2	STGB	27.8	0	791.8
3	STGB	32.3	0	819.818
4	STGB	16.4	0	759.547
6	STGB	60	0	0
5	ATGB	32.3	10	852.58

0° and 60°, bi-crystalline structure of Zr transforms back to single crystal, and properties corresponds to bulk materials.

It can be observed from the GB energies in Table 2 that despite the same misorientation angle of 32.3°, ATGB configuration has higher GB energies as compared to corresponding STGB. This variation between GB energies in STGB and ATGB configuration is attributed to the ordered and disordered atomic configurations, respectively.

3.2. Effect of grain boundary on crack tip behaviour

As discussed in the previous section, two separate crack orientations were considered to study the effect of GB stresses on the crack tip behaviour. The schematic of simulation box along with the centrally embedded crack with respect to GB planes and boundary conditions are shown in Fig. 4. Crack length aligned perpendicular (Fig. 4a) and parallel (Fig. 4b) to GB plane will be referred as type-I and type-II in the preceding sections.

First set of simulations were performed with a constant crack length, but with varying distance between the two GB planes, which is referred as GB-15, GB-30 and GB-60. Here numerical value designates the distance in angstrom (Å) between the crack tip and GB plane. These set of simulations were performed with type-I crack. In order to capture the effect of GB on the crack tip behaviour, stresses in the region encircled in Fig. 4a (crack tip) was captured during the tensile deformation. Crack tip stresses were measured in a small spherical region of radius 3 Å around the crack tip. Stress strain response perpendicular to the crack surfaces are plotted in Fig. 5 that corresponds to average stress values experienced by group of atoms in front of crack tip. Statistical distribution of temperature over this small number of atoms in the confined group shown by red circles in Fig. 4, induces stress fluctuations in response plotted in Fig. 5. In order to perform the comparative analysis of the effect of GB on the crack tip stresses in GB-15, GB-30 and GB-60 configurations, the normalized value of stresses were used in Figs. 5 and 8. The normalized stress means that the per atom stress values have been divided by a common factor of 10^9eV/Å^3 to make the quantity dimensionless. The plots in Fig. 5, thus do not indicate the actual stress values, but a comparative picture of the per atom stresses at the crack tip in different configurations. Lower value of stresses was observed at the crack tip in Fig. 5, while simulations were performed with GB planes in closer vicinity of crack tips (GB-15), as compared to GB-30 and GB-60 respectively.

It can be inferred from this subsection that presence of GB in close vicinity to crack tip helps in mitigating the higher crack tip opening stresses, hence maximum reduction in crack tip stresses were observed in GB -15 and minimum in GB-60. It can also be inferred from the trend plotted in Fig. 5 that simulations performed

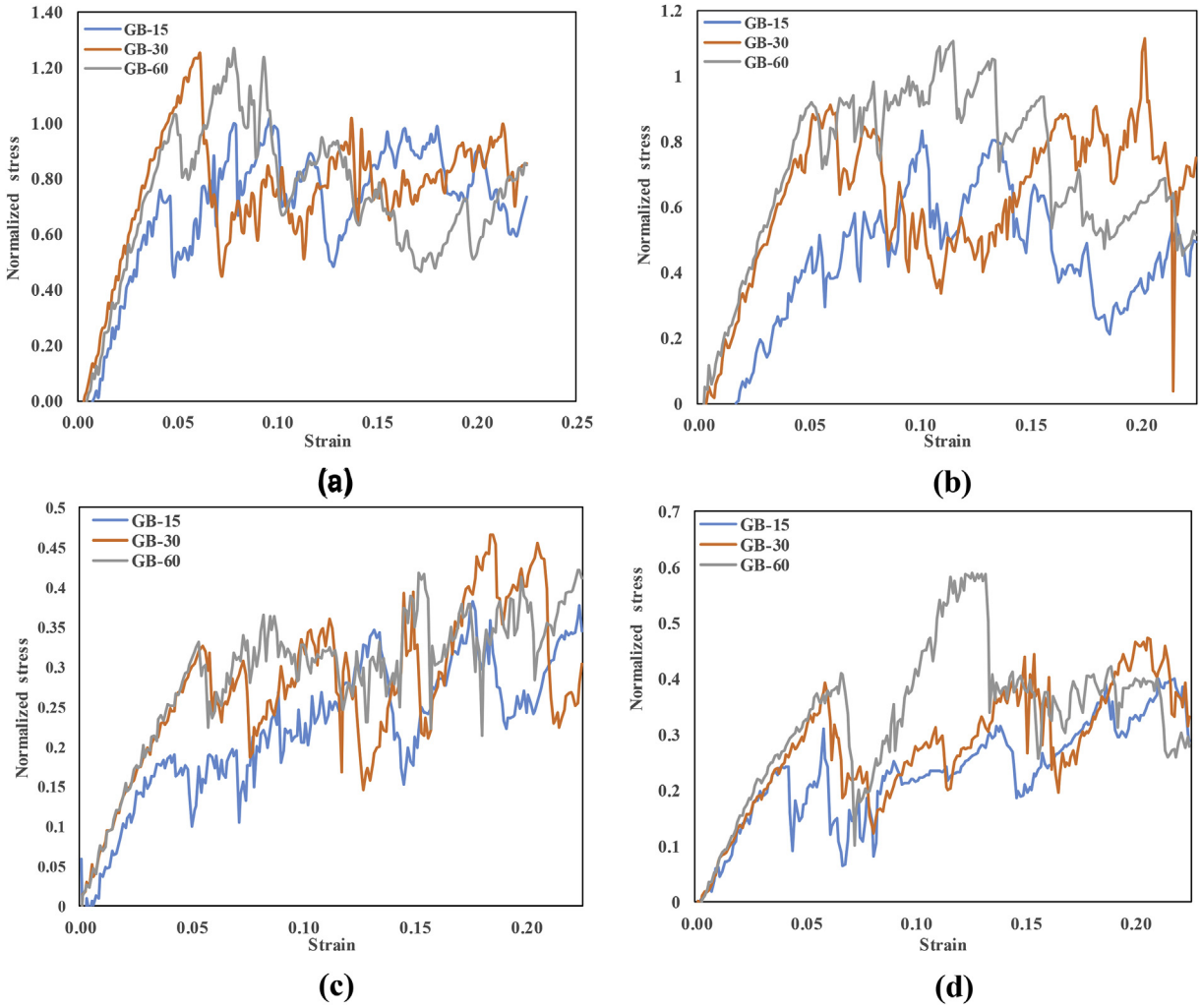

Fig. 5. Normalized crack tip stresses for bi-crystal with misorientation angle (a) 32.3° (STGB) (b) 32.3° (ATGB with inclination = 10°) (c) 27.8° (d) 16.4° (Stress values were divided by 10^9eV/Å^3 to normalized).

with lower misorientation angles of 16.4° and 27.8° have lower values of crack tip stresses as compared to simulations performed with a misorientation angle of 32.3° (symmetrical and asymmetrical). This trend is consistent with the grain boundary energy, higher energy GB configurations have higher values of stresses at the crack tip and vice-versa. This phenomenon was earlier explained as disclination shielding in the article [17]. Disclination shielding occurs when the dislocation sources transform from crack tip to grain boundary. The equilibrium structure of grain boundary gets disturbed and stresses at the grain boundary increases that shifts the emission of dislocations from crack tip to grain boundary. In order to capture the deformation and emission of dislocations in bi-crystal of Zr, snapshots of the simulation box for each case at different strain values 'ε' are shown in Fig. 6 and Fig. 7. The trend in all the misorientation angle with respect to distance from the crack tip was almost same, hence only snapshots corresponding to misorientation angle of 32.3° and 16.4° are shown in Figs. 6 and 7, respectively.

It can be depicted from the deformation morphology shown in Figs. 6 and 7 that twinning/dislocations emits from the crack tip, while the simulation was performed with GB-60 configuration that corresponds to maximum distance of 60 Å between crack tip and GB plane. On the other hand, shift in the region of deformation from the crack tip to GB plane was observed in simulations that was performed with GB-15 and GB 30 configurations. This shift in trend is in good agreement with the crack tip stresses plotted in Fig. 5. In the simulations performed with the GB-60 configuration, role of the grain boundary was to act as an obstacle to dislocation movement, whereas in GB-30, the grain boundary is in close vicinity of the crack tip, hence effectively shields the crack tips from higher stresses, and shifts the emission of dislocation to the GB plane. Overall, the reduction in crack tip stresses helps in enhancing the strength of bi-crystalline Zr that corresponds to GB-15 configuration. Reduction in crack tip stresses occurs as the dislocation emission shifts from the crack tip to the grain boundaries. This shifts the failure initiation from the crack tip, and thus enhances the fracture strength of the bi-crystals. Change in crack length in conjunction with dislocation length in each simulation performed with GB-15, GB-30 and GB-60 are tabulated in Table 3.

It can be observed from Table 3 that a positive increment in the crack length was observed, while the crack tip was simulated at a distance of 15 Å (GB-15) from the GB plane, whereas crack blunting was observed in all other cases. A dip in crack tip stresses was observed in GB-15, which was associated with suppression of dislocation emission from crack tips as compared to GB-30 and GB-60 configurations. Suppression of dislocation emissions from the crack tip in GB-15, leads to bond breaking and increment in crack length, whereas in GB-30 and GB-60 configurations, higher

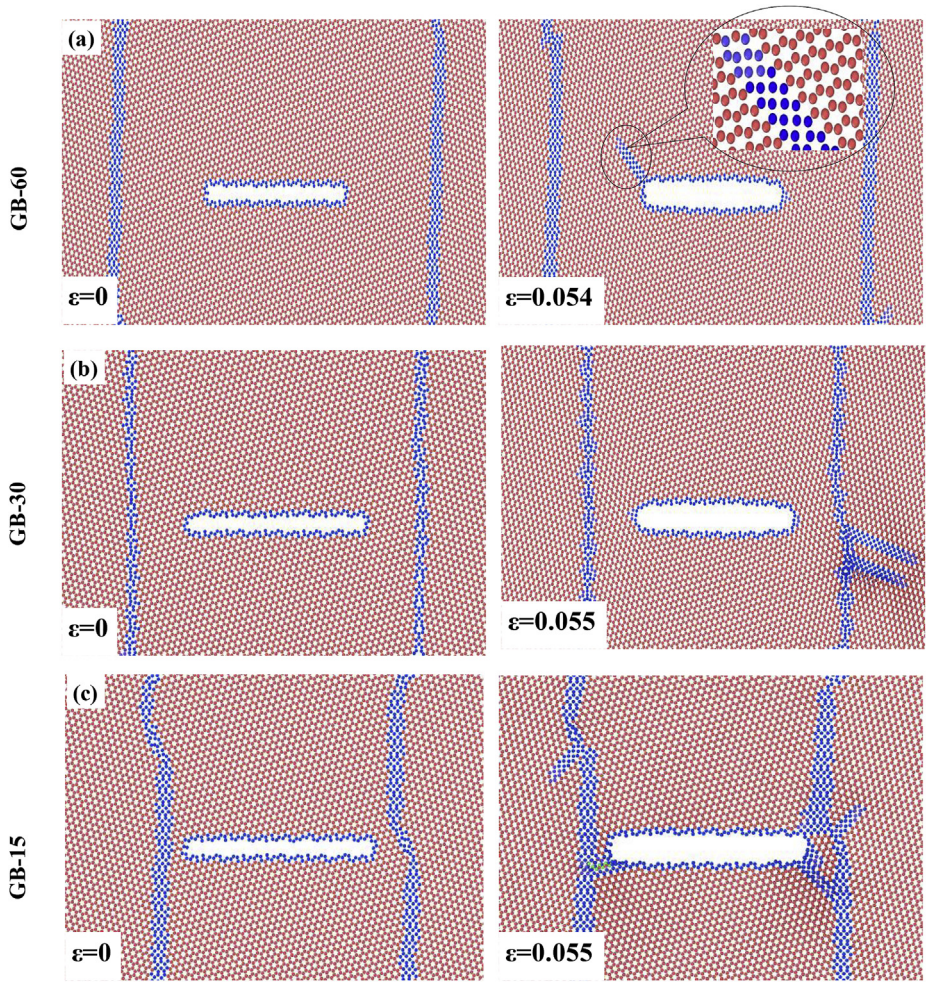

Fig. 6. Snapshots of the simulation box containing STGB ($2\theta = 32.3°$) in conjunction with centrally embedded crack of type-I for three different configuration (a) GB-60 (b) GB-30 (c) GB-15 (atoms are coloured according to common neighbour analysis-CNA-red depict perfect hcp Zr and blue depict the crystal structure other than hcp). (For interpretation of the references to colour in this figure legend, the reader is referred to the Web version of this article.)

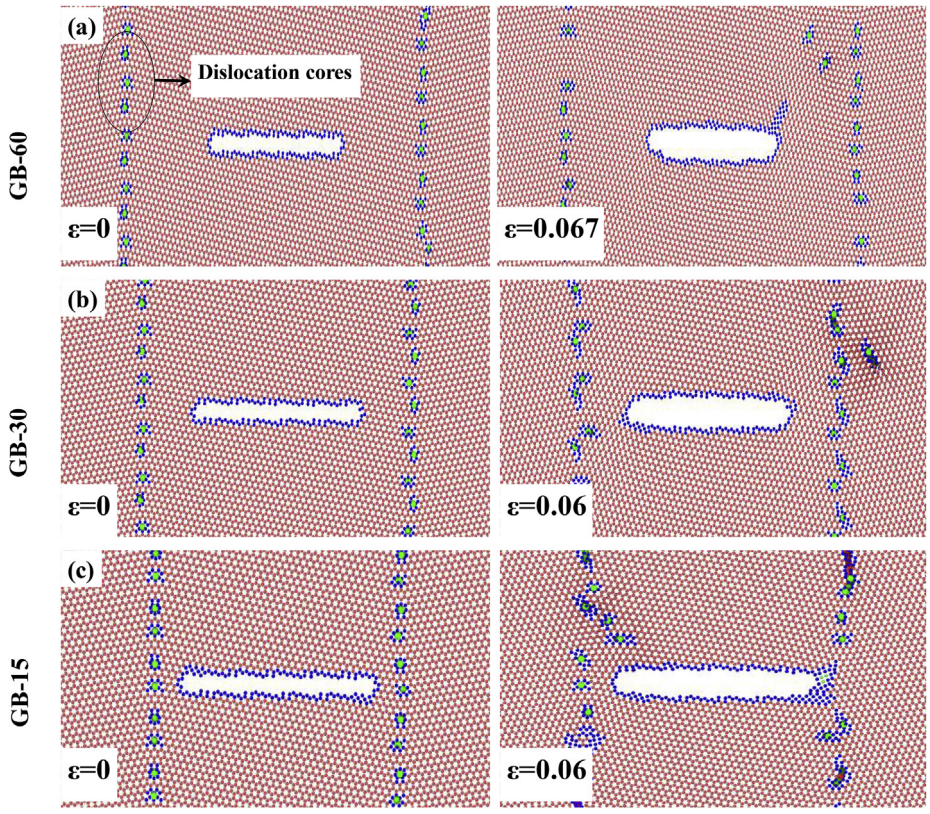

Fig. 7. Snapshots of the simulation box containing STGB ($2\theta = 16.4^{\circ}$) in conjunction with centrally embedded crack of type-I for three different configuration (a) GB-60 (b) GB-30 (c) GB-15.

dislocation emissions from the crack tips helps in blunting the crack propagation. Thus crack tip behaviour is dependent on its distance from the grain boundary plane. Maximum increment in the crack length was observed in ATGB configuration placed at a distance of 15 Å from the crack tip.

Next set of simulations were performed with crack parallel to the grain boundary plane referred as type −II in Fig. 4b. Normalized crack tip stresses as a function of strain is plotted in Fig. 8. In contrast to type-I crack, no effect of shielding was observed in Fig. 8, with type-II crack. This kind of behaviour can be attributed to the orientation of the crack tip with respect to the grain boundary. Since, grain boundary no longer lies ahead of the crack tip, the disclination shielding was absent and, hence no significant variation in the failure morphology as well as crack tip stresses was observed in any of the bi-crystals, containing type-II cracks. Snapshots of the simulation box at the time of onset of dislocation or twinning in ATGB containing misorientation and inclination angle of 32.3° and 10° are shown in Fig. 9. It can be seen in Fig. 9 that in all configurations GB-15, GB-30 and GB-60, deformation of the bi-crystal initiates from the crack tip, and it was not affected by the presence of GB plane. Change in crack length in conjunction with dislocation length with type-II cracks are tabulated in Table 3.

As compared to dislocation length observed with type-I cracks, no significant variation in the crack length was observed with type-II cracks, since there is no influence of the grain boundary on the crack tip stresses.

3.3. Effect of crack length on fracture properties of Zr bi-crystals

In order to study the effect of crack length on the fracture behaviour of Zr bi-crystals, three different crack lengths were generated in the bi-crystals containing STGB and ATGB configurations with misorientation and inclination angle of 32.3° and 10°, respectively. It can be observed from the stress-strain response plotted in Fig. 10 and Fig. 12 that maximum value of stresses under mode-I loading corresponds to the minimum crack length and vice versa. Snapshots of the simulation box at the onset of plastic deformation in STGB and ATGB configuration are shown in Fig. 11 and Fig. 13, respectively. It can be observed in Fig. 10 that hardening was observed with crack length of 60 Å, while the twin dislocation emitting from the crack tip interacts with the STGB structure as shown in Fig. 11 at $\varepsilon = 0.046$. On the other hand, simulations performed with the crack length of 90 Å, the emission of twin dislocations shifts from crack tip to non-equilibrium boundaries. In case of the bi-crystal with a crack length of 120 Å, no dislocations emerge from the crack tip, as the crack tip merges into the grain boundary. After subjecting bi-crystal with crack length of 120 Å to tensile deformation, the equilibrium structure of the STGB undergoes change and triggers emission of dislocation from GB plane, instead of crack tip.

In case of ATGB configurations with a crack length of 60 Å, a twin dislocation emerges from the crack tip at $\varepsilon = 0.051$ as depicted in Fig. 13. A slight hardening can be seen corresponding to the strain values in the stress-strain response plotted in Fig. 12. In case of bi-crystal with a crack length of 90 Å, the grain boundary transforms into adjacent non equilibrium configuration and emits a twin dislocation. In case of the bi-crystal with a crack length of 120 Å, no dislocation emerges from the crack tip, as the crack tip merges into the grain boundary. Upon tensile loading, a significant distortion in the grain boundary structure can be observed in this case.

In the end of this subsection, it can be concluded that deformation in the bi-crystal of Zr triggers from the crack tip and GB

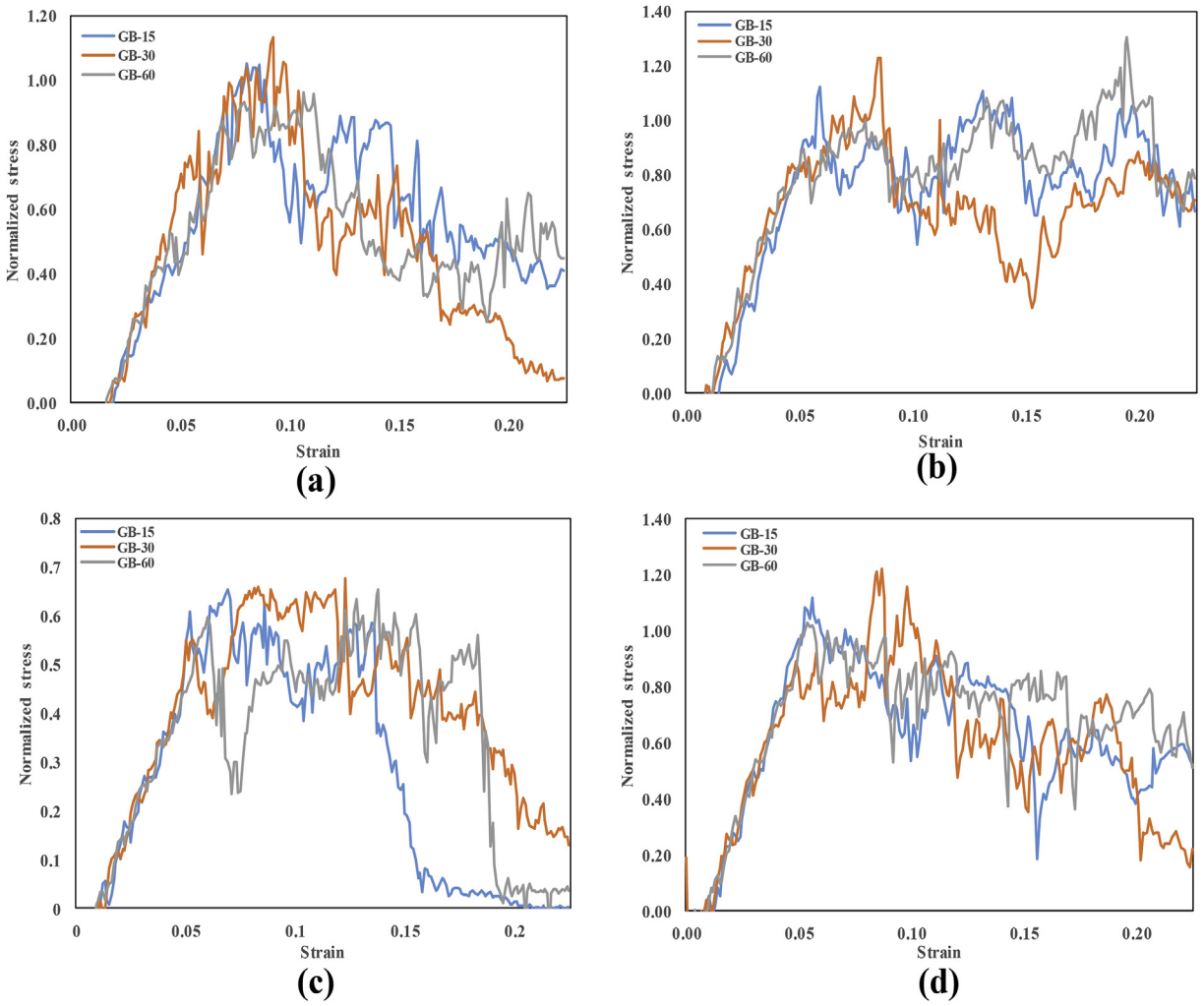

Fig. 8. Normalized crack tip stresses for bi-crystal with misorientation angle (a) 32.3° (b) 32.3° and inclination = 10° (c) 27.8° (d) 16.4° (type −II crack configuration) (Stress values were divided by 10^9eV/Å^3 to normalized).

Table 3
Dislocation length, change in crack length for different type of GB configurations.

Distance of crack tip from grain boundary (Å)	Dislocation length (Å)		Misorientation(2θ) And Inclination(Ø) angle	Initial crack length (Å)	Final crack length (Å)	Initial crack length (Å)	Final crack length (Å)
	Type I	Type II		Type I		Type II	
15	430	1202	2θ = 32.3°,Ø = 0°	90	94	63.88	64.86
30	3344	238.36		90	88.9	64.63	63.55
60	361	1283.32		90	89.38	62.99	62.1
15	598.21	1813	2θ = 32.3°,Ø = 10°	90	106.9	61.13	74.6
30	1020.37	1064		90	85	62.88	64.74
60	970.394	1914		90	90	62.73	61.04
15	956.671	1864	2θ = 27.8°,Ø = 0°	90	93	63.7	64.48
30	1878	2307		90	90	63.8	61.13
60	2846.94	2287		90	89	64.67	68.08
15	2512	1925	2θ = 16.4°,Ø = 0°	90	94.47	63	66.9
30	2898	2741		90	94.8	64.8	57.3
60	2388	2923		90	93.42	63.2	65.98

structure for small and large crack lengths, respectively. This trend is consistent with the results obtained with type-I crack simulated with GB-15, GB-30 and GB-60 configurations. As the crack tip interacts with the GB atoms, the deformation triggers from the STGB or ATGB configuration instead of crack tip atoms, whereas the opposite trend was observed with small crack lengths.

3.4. Crack tip behaviour in irradiated bi-crystal of Zr

In order to study the effect of irradiation on the fracture behaviour of Zr bi-crystals, two set of simulations were carried out with the STGB and ATGB configurations containing misorientation and inclination angle of 32.3° and 10°, respectively. All the

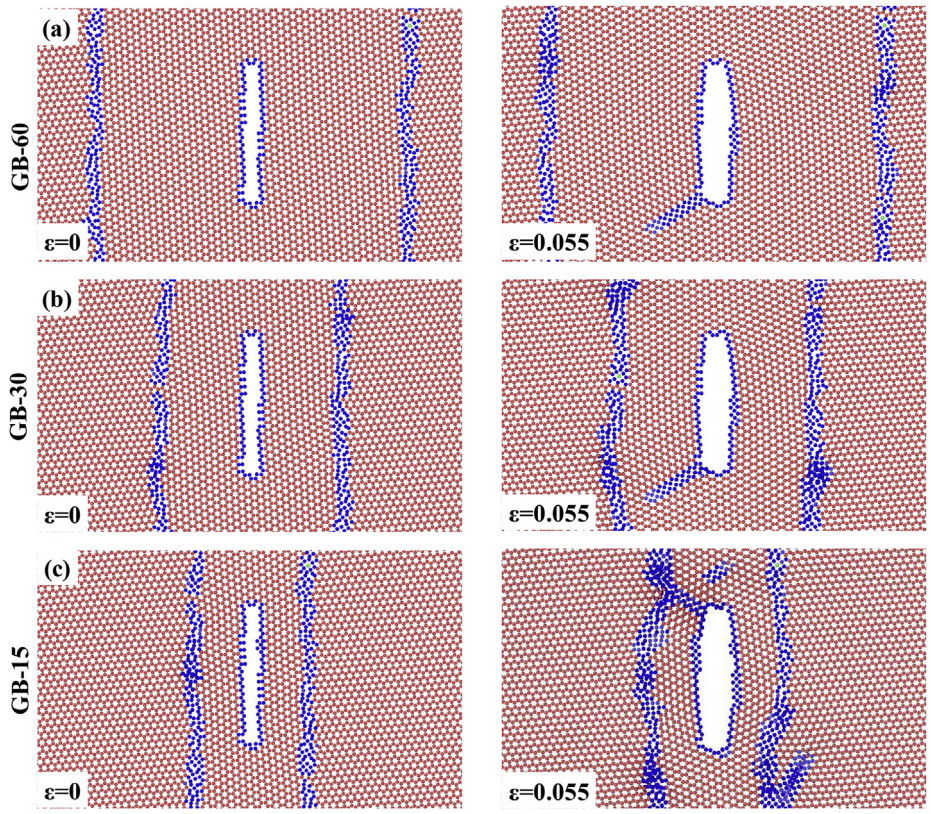

Fig. 9. Snapshots of the simulation box containing ATGB ($2\theta = 32.3^\circ$ $\emptyset = 10^\circ$) in conjunction with centrally embedded crack of type-I for three different configuration (a) GB-60 (b) GB-30 (c) GB-15 (atoms are coloured according to common neighbour analysis-CNA-red depict perfect hcp Zr and blue depict the crystal structure other than hcp). (For interpretation of the references to colour in this figure legend, the reader is referred to the Web version of this article.)

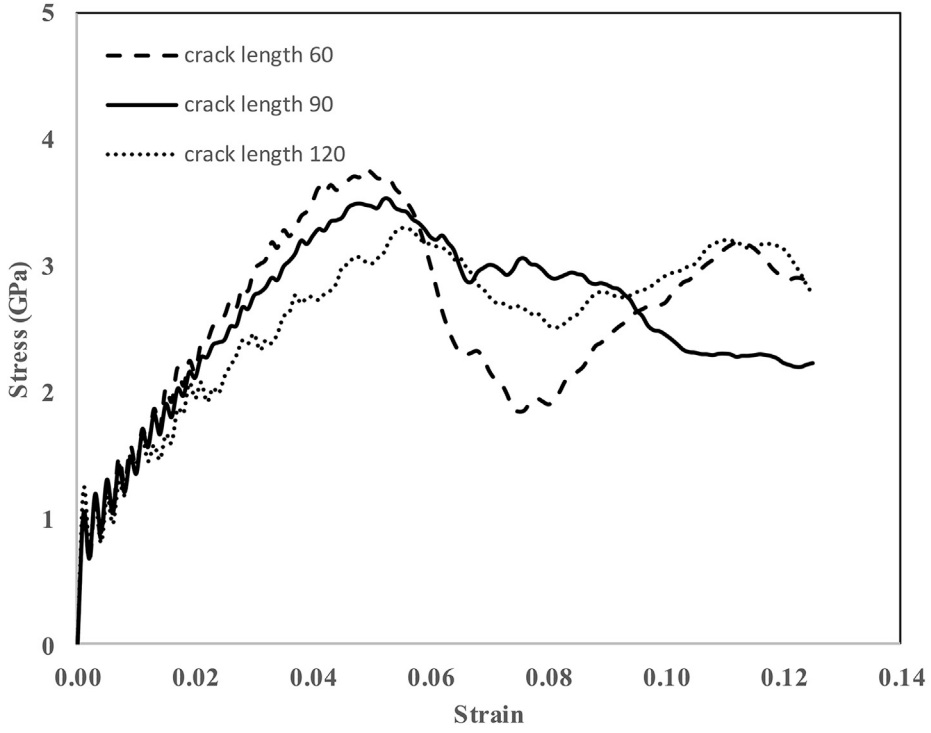

Fig. 10. Stress-strain response for a symmetric bi-crystals with misorientation = 32.3° containing a central crack of length 60, 90 and 120 Å respectively.

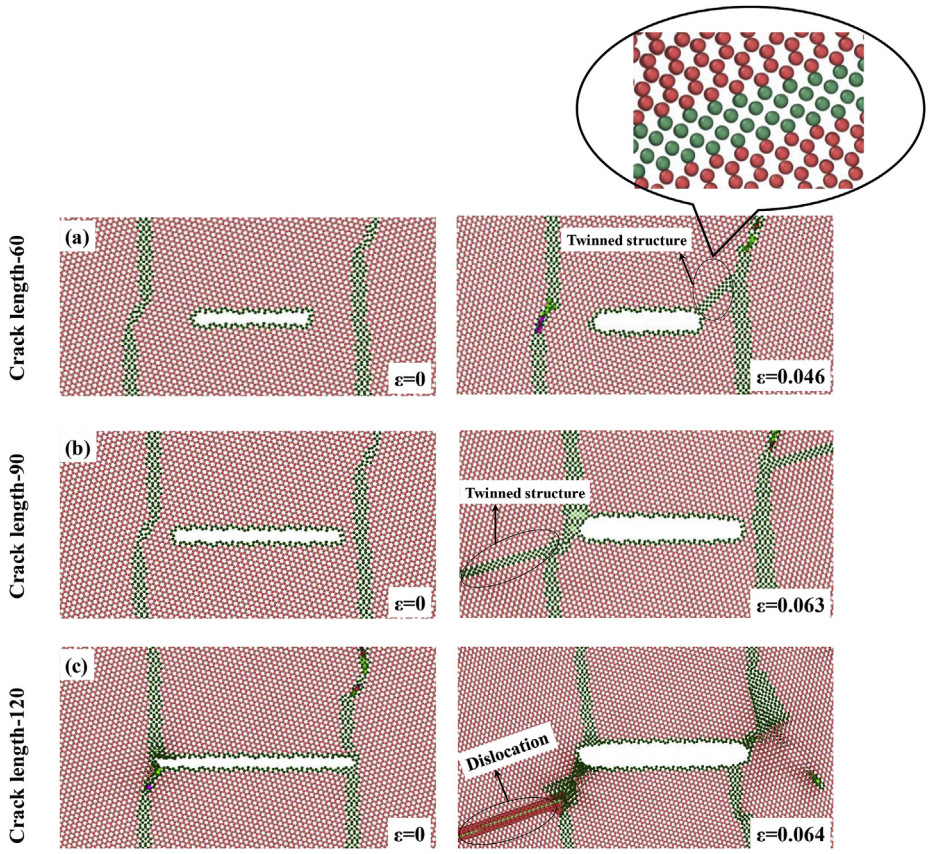

Fig. 11. Snapshot of the simulation box showing failure morphology in a symmetrical bi-crystal (misorientation = 32.3°) with change in crack length. (atoms are coloured according to dislocation analysis-red and green depict perfect hcp Zr and atoms other than hcp). (For interpretation of the references to colour in this figure legend, the reader is referred to the Web version of this article.)

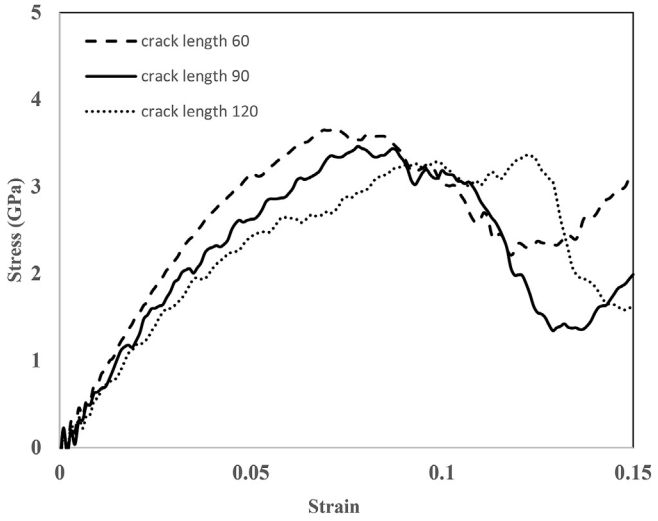

Fig. 12. Stress-strain response for an asymmetric bi-crystal with misorientation and inclination angle of 32.3° and 10°, respectively for the crack length of 60, 90 and 120 Å.

simulations were performed with two crack lengths of 90 Å and 120 Å. Irradiation induced defects were studied with respect to their quantity and spatial distribution. In order to generate different number of irradiation induced point defects in the simulation box, multiple PKA's with kinetic energy in the range of 2 keV were simulated in the vicinity of crack, without creating any damage to the crack profile. Later on the same atomic configurations containing point defects were subjected to uni-axial tensile loading in the direction perpendicular to the crack plane.

Initially, simulations were performed to study the effect of spatial distribution of irradiation induced defects on the ultimate tensile strength (UTS) of bi-crystalline Zr. The number of defects were kept constant with respect to each misorientation angle, but their spatial distribution was varied in the simulation box with the help of random number generator. All the simulations were performed at a temperature of 1 K. This temperature/thermal distribution over the atoms in the simulation box was performed with the help of random number generator in LAMMPS. These random number generators help in assigning temperature/velocity values over the atoms with an average of 1 K for the whole simulation box. In all the simulations, Gaussian distribution was used to assign temperature/velocity over the atoms. As temperature was distributed randomly over the atoms, hence, energy of PKA atoms selected in the simulation box also got affected. In order to compensate the random distribution of temperature over the atoms, multiple simulations were run with different set of random numbers for each set of irradiation-induced defects. Switching random number alters the distribution of thermal component over the same PKA atoms, which ultimately changes the spatial distribution and number of defects generated in the simulation box. In order to capture the effect of spatial distribution of defects around the crack tip, simulations generating same number of defects were considered for UTS calculations. It has been attempted in this section of the article to demonstrate that on keeping the number of defects approximately same, but changing their position with respect to

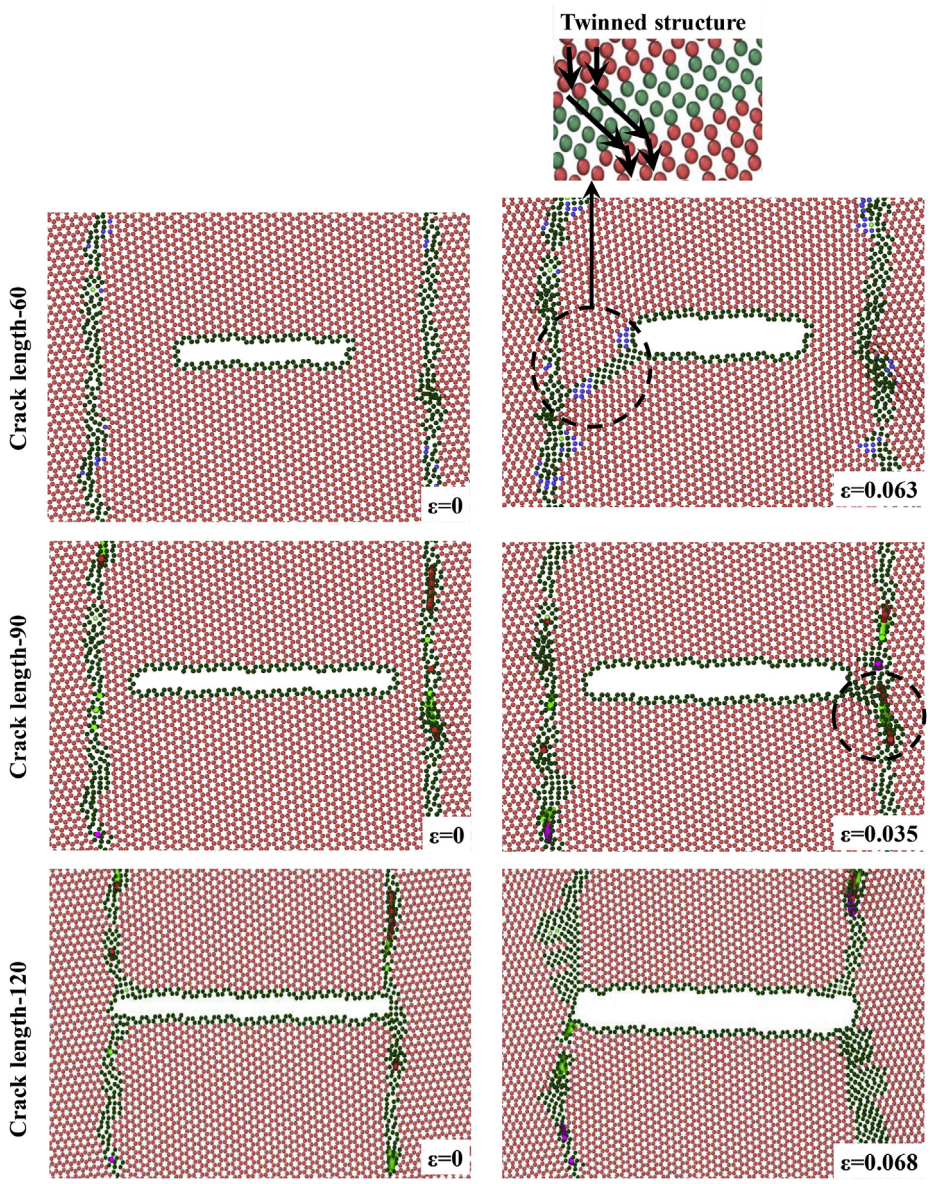

Fig. 13. Snapshot of the simulation box showing failure morphology in an asymmetrical bi-crystal (misorientation = 32.3°, inclination = 10°) with change in crack length. (atoms are coloured according to dislocation analysis-red depict perfect hcp Zr and green depict the crystal structure other than hcp). (For interpretation of the references to colour in this figure legend, the reader is referred to the Web version of this article.)

the grain boundaries and crack front, the UTS changes. It can be observed from the trend plotted with the error bars in Fig. 14 (STGB) and Fig. 15 (ATGB) that spatial distribution of defects have some effect on the UTS of bi-crystalline Zr. Pristine bi-crystalline Zr corresponds to non-irradiated material.

It can be observed from Figs. 14 and 15 that UTS of bi-crystalline Zr containing point defects increases as compared to non-irradiated bi-crystal. The spatial distribution has significant effect on the strength of bi-crystals of Zr, which is attributed to the fact that dislocation/twinning has different probability of interaction with these spatial distributions. The change in spatial distribution/position of the defects leads to a change in the path of interaction of the moving twins and dislocation with the defects.

Effect of number of irradiation induced defects on the UTS of bi-crystalline Zr is plotted in Fig. 16 and Fig. 17 for STGB and ATGB configurations, respectively. In these simulations the distance between the grain boundary planes were maintained constant at 120 Å. It can be observed from Figs. 16 and 17 that irrespective of the crack length, strength of bi-crystalline Zr improved up to certain number of irradiation induced point defects, but deteriorates for higher range of defects. It can be further inferred from the trend plotted in Figs. 16 and 17 that higher number of defects above 200, severely damages the material, which eventually reduces the strength. Overall reduction in the strength of the material due to higher number of irradiation induced defects (>200), compensates and mitigates the effect of strengthening observed in fewer number of defects. It can be observed from Figs. 16 and 17 that trend is almost same irrespective of crack length and grain boundary configuration, that is STGB or ATGB. The increase in the strength at lower number of irradiation induced defects can be attributed to the increase in probability of interaction of the dislocations with these defects.

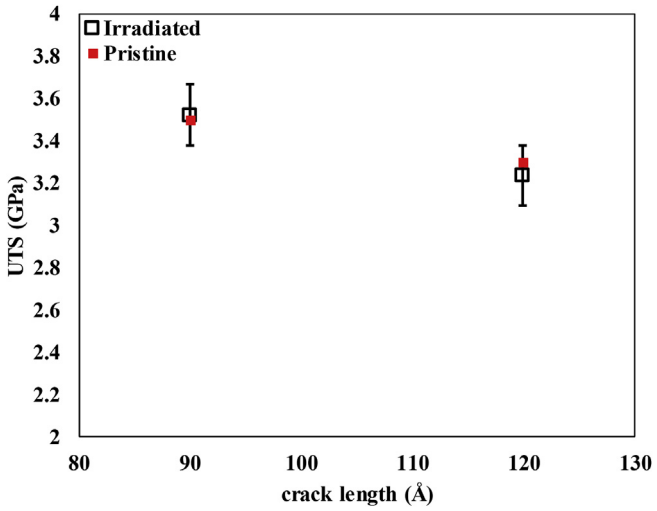

Fig. 14. UTS of bi-crystalline Zr containing two different types of crack lengths for STGB ($2\theta = 32.3°$).

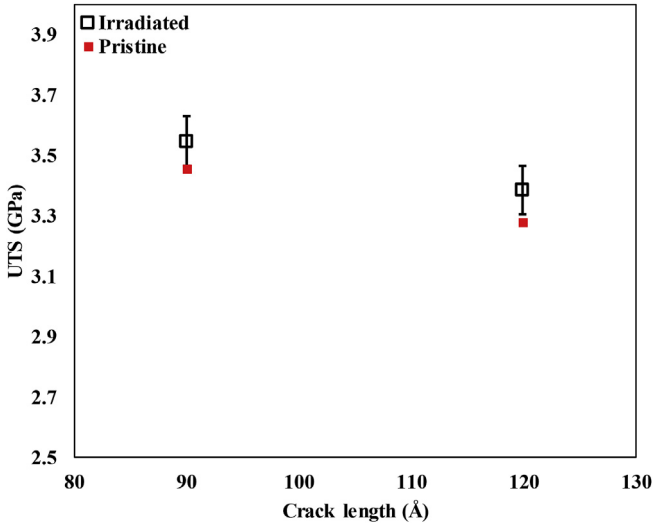

Fig. 15. UTS of bi-crystalline Zr containing two different types of crack lengths for ATGB ($2\theta = 32.3°$, $\emptyset = 10°$).

It can be observed from Fig. 18 that twin dislocations that emerge from the grain boundary interact with the point defects as they advance into the crystal. The interaction of the moving dislocations with the point defects causes a hurdle in the movement of the dislocations, resulting in strengthening, as depicted in Figs. 16 and 17. It can be seen that the increase in UTS is directly proportional up to a certain number of defects only. Any further increment in the number of these defects starts mitigating the strength of the bi-crystalline Zr. It can be seen in Fig. 18 that as the number of point defects increases from 30 to 80, the moving dislocations interact with more number of point defects, thus further increasing the strength and no damage was caused to the grain boundary plane. However, it can be seen that when the number of point defect reaches 280, there was damage in the grain boundary configuration. This, in turn, leads to weakening of the grain boundary and the bi-crystal. This causes an overall decrease in the strength, despite the presence of a higher number of point defects.

Another important feature present in irradiated bi-crystals was the presence of dislocation loops. It can be seen in Fig. 19, that upon tensile loading, vacancy type dislocation loop was formed just after the cascade, aligned with the prismatic plane with a burger vector $b = 1/2(0\text{–}110)$. It has been reported in the work of Tian et al. [27] and Varvenne et al. [28] that vacancy type dislocation loops are stable in prismatic plane at lower irradiation energy, which is the case simulated in the simulation box. On further loading, the loop becomes unstable and disintegrates.

4. Conclusion

It can be concluded from the MD based simulations that interaction of crack tip, dislocations and grain boundaries play a significant role in determining fracture behaviour and strength of bi-crystalline Zr. Spatial positioning of GB plane with respect to the crack tip was predicted to have significant effect on the deformation mechanism of bi-crystalline Zr. Opening stresses at the crack tip was reduced in near vicinity of the GB plane for type-I cracks, but no such effect of GB was observed in type-II crack. Simulations performed with irradiated bi-crystals predicted an improvement in the strength up to a certain number of point defects, but after crossing that limit strength of bi-crystalline Zr starts mitigating.

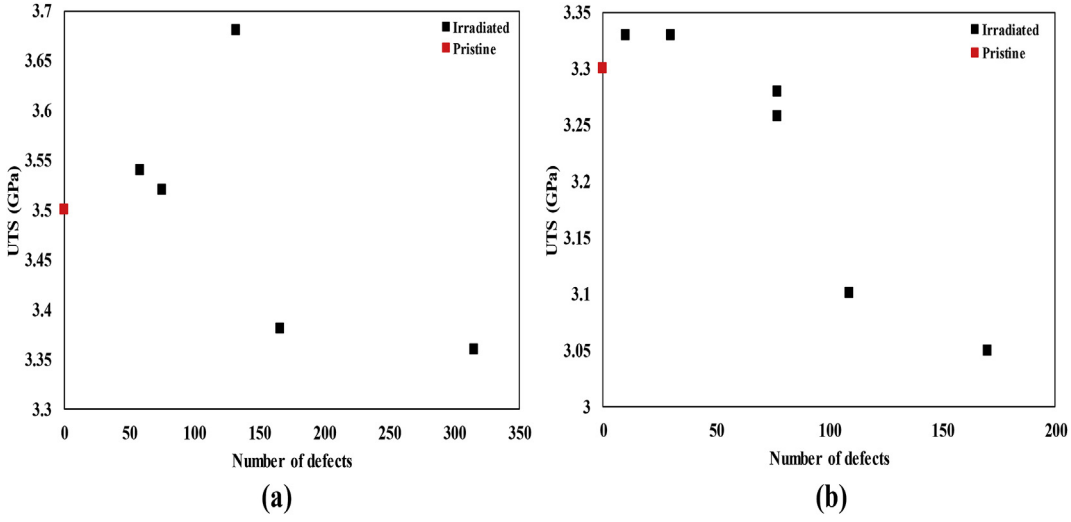

Fig. 16. UTS versus number of defect symmetric $2\theta = 32.3°$ for crack length (a) 90 Å (b) 120 Å

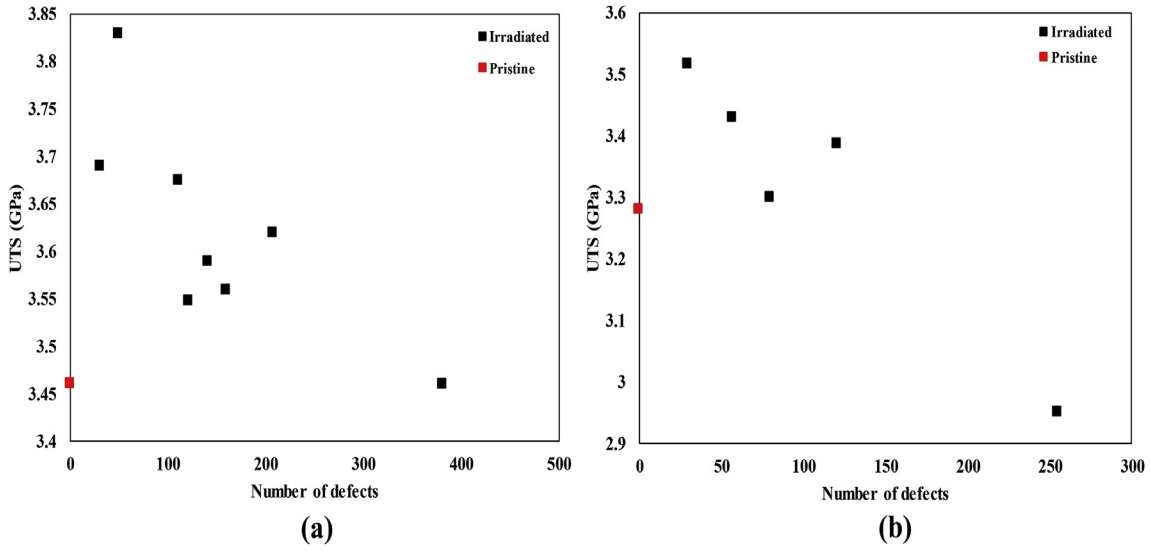

Fig. 17. UTS versus number of defect symmetric $2\theta = 32.3^{\circ}$, $\emptyset = 10^{\circ}$ for crack length (a) 90 Å (b) 120 Å.

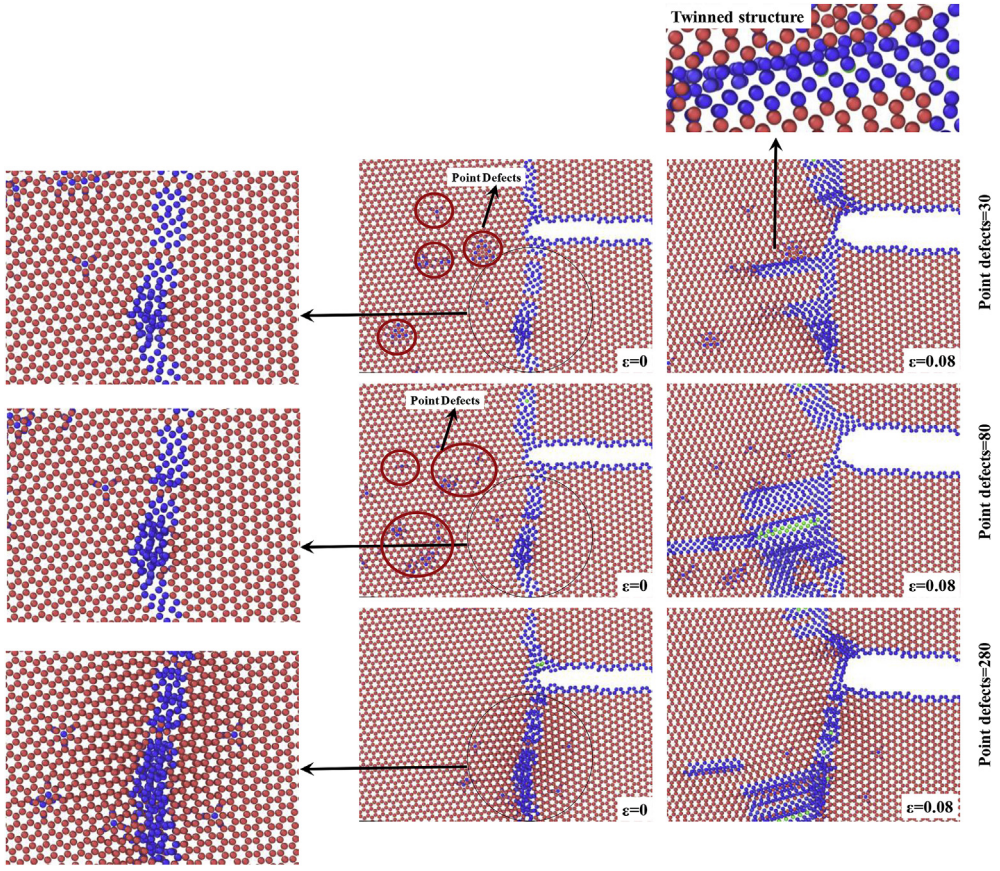

Fig. 18. Snapshot of the simulation box showing failure morphology in an irradiated asymmetrical bi-crystal (misorientation = 32.3°, inclination = 10°) with crack length = 120 Å (atoms are coloured according to CNA-red depict perfect hcp Zr and blue depict the crystal structure other than hcp). (For interpretation of the references to colour in this figure legend, the reader is referred to the Web version of this article.)

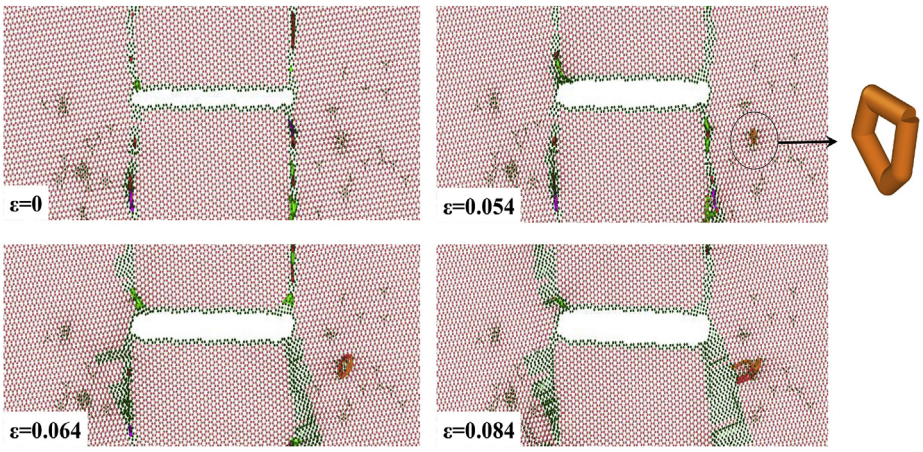

Fig. 19. Snapshot of the simulation box showing failure morphology in an irradiated asymmetrical bi-crystal (misorientation = 32.3°, inclination = 10°) with crack length = 120 Å (atoms are coloured according to dislocation analysis-red depict perfect hcp Zr and green depict the crystal structure other than hcp, the enlarged orange loop is vacancy type dislocation loop). (For interpretation of the references to colour in this figure legend, the reader is referred to the Web version of this article.)

Data availability

The raw/processed data required to reproduce these findings cannot be shared at this time due to technical or time limitations.

Acknowledgement

We would like to thank BRNS, Department of Atomic Energy, India (Project No. DAE-984-MID) for providing financial support to this project.

Appendix A. Supplementary data

Supplementary data to this article can be found online at https://doi.org/10.1016/j.jnucmat.2019.151739.

References

[1] E.O. Hall, The deformation and ageing of mild steel: III discussion of results, Proc. Phys. Soc. B 64 (1951) 747.
[2] N.J. Petch, The cleavage strength of polycrystals, J. Iron Steel Inst. 174 (1953) 25–28.
[3] A.H. Chokshi, A. Rosen, J. Karch, H. Gleiter, On the validity of the hall-petch relationship in nanocrystalline materials, Scr. Metall. 23 (1989) 1679–1683.
[4] G.E. Fougere, J.R. Weertman, R.W. Siegel, S. Kim, Grain-size dependent hardening and softening of nanocrystalline Cu and Pd, Scr. Metall. Mater. 26 (1992) 1879–1883.
[5] P.G. Sanders, J.A. Eastman, J.R. Weertman, Elastic and tensile behavior of nanocrystalline copper and palladium, Acta Mater. 45 (1997) 4019–4025.
[6] R.A. Masumura, P.M. Hazzledine, C.S. Pande, Yield stress of fine grained materials, Acta Mater. 46 (1998) 4527–4534.
[7] A.S. Khan, H. Zhang, L. Takacs, Mechanical response and modeling of fully compacted nanocrystalline iron and copper, Int. J. Plast. 16 (2000) 1459–1476.
[8] J. Schiøtz, T. Vegge, F.D. Di Tolla, K.W. Jacobsen, Softening of nanocrystalline metals at very small grain sizes, Nature (London) 391 (1998) 561–563.
[9] V. Yamakov, D. Wolf, S.R. Phillpot, A.K. Mukherjee, H. Gleiter, Deformation mechanism crossover and mechanical behaviour in nanocrystalline materials, Philos. Mag. Lett. 83 (2003) 385–393.
[10] J. Schiøtz, K.W. Jacobsen, A maximum in the strength of nanocrystalline copper, Science 301 (2003) 1357–1359.
[11] T. Shimokawa, A. Nakatani, H. Kitagawa, Grain-size dependence of the relationship between intergranular and intragranular deformation of nanocrystalline Al by molecular dynamics simulations, Phys. Rev. B 71 (2005) 224110.
[12] J.M. Hodge, R.D. Manning, H.M. Reichhold, The effect of ferrite grain size on notch toughness, Trans. Am. Inst. Min. Metall. Eng. 185 (1949) 233–240.
[13] N. Tsuji, S. Okuno, Y. Koizumi, Y. Minamino, Toughness of ultrafine grained ferritic steels fabricated by ARB and annealing process, Mater. Trans. 45 (2004) 2272–2281.
[14] M. Tanaka, N. Fujimoto, K. Higashida, Fracture toughness enhanced by grain boundary shielding in submicron-grained low carbon steel, Mater. Trans. 49 (2008) 58–63.
[15] S.J. Noronha, D. Farkas, Effect of dislocation blocking on fracture behavior of Al and α-Fe: a multiscale study, Mater. Sci. Eng. A 365 (2004) 156–165.
[16] X. Zeng, A. Hartmaier, Modeling size effects on fracture toughness by dislocation dynamics, Acta Mater. 58 (2010) 301–310.
[17] T. Shimokawa, M. Tanaka, K. Kinoshita, K. Higashida, Roles of grain boundaries in improving fracture toughness of ultrafine-grained metals, Phys. Rev. B 83 (2011) 214113.
[18] M. Griffiths, D. Sage, R.A. Holt, C.N. Tome, Determination densities in HCP metals from X-ray diffraction line-broadening analysis, Metall. Mater. Trans. A 33A (2002) 859–865.
[19] J.E. Bailey, Electron microscope studies of dislocations in deformed zirconium, J. Nucl. Mater. 7 (3) (1962) 300–310.
[20] M. Rafiqe, N. Afzal, R. Ahmad, S. Ahmad, I.M. Ghauri, Mechanical behaviour of low-dose neutron-irradiated polycrystalline zirconium, Radiat. Eff. Defects Solids 167 (4) (2012) 289–297.
[21] Priti Kotak Shah, J.S. Dubey, R. S Shriwastaw, M.P. Dhotre, A. Bhandekar, K.M. Pandit, S. Anantharaman, R.N. Singh, J.K. Chakravartty, Fracture Toughness of irradiated Zr-2-5Nb pressure tube from Indian PHWR, J. Nucl. Mater. 458 (2015) 319–325.
[22] K. Kapoor, V.K. Saxena, S.V. Swamy, N. Saratchandran, G. Malakondaiah, B.P. Kashyap, Measurement of Fracture Properties of Zr-2.5 Wt.% Nb pressure tube material and effect of trace impurities, Pract. Fail. Anal. 2 (3) (2002) 65–70.
[23] D.D. Himbeault, C.K. Chow, M.P. Puls, Deformation behaviour of irradiated Zr-2.5Nb pressure tube material, Metall. Mater. Trans. A 25 (1) (1994) 135–145.
[24] M.I. Medelev, G.J. Ackland, Development of an interatomic potential for the simulation of phase transformations in zirconium, Philos. Mag. Lett. 87 (5) (2007) 349–359.
[25] S. Plimpton, Fast parallel algorithms for short range molecular dynamics, J. Comput. Phys. 117 (1995) 1–19.
[26] A. Stukowski, Visualization and analysis of atomistic simulation data with OVITO-the open visualization tool, Model. Simul. Mater. Sci. Eng. 18 (2010), 015012.
[27] Wei Zhou, Jiting Tian, Jian Zheng, Jianming Xue, Shuming Peng, Dislocation-enhanced experimental-scale vacancy loop formation in hcp Zirconium in one single collision cascade, Sci. Rep. 6 (2016) 21034.
[28] Celine Varvenne, Olivier Mackain, Emmanuel Clouet, Vacancy clustering in zirconium: an atomic scale study, Acta Mater. 78 (2014) 65–77.
[29] Divya Singh, Avinash Parashar, Effect of symmetrical and asymmetrical tilt grain boundaries on radiation induced defects in zirconium, J. Phys. D Appl. Phys. 51 (26) (2018) 265301.
[30] Divya Singh, Avinash Parashar, Rajeev Kapoor, Apu Sarkar, A. Kedharnath, Effect of symmetrical and asymmetrical tilt grain boundaries on the tensile deformation of zirconium bi-crystals: a MD based study, J. Mater. Sci. 54 (2019) 3082–3095.
[31] Divya Singh, Pankaj Sharma, Sahil Jindal, Prince Kumar, Piyush Kumar, Avinash Parashar, Atomistic simulations to study crack tip behaviour in single crystal of bcc Niobium and hcp Zirconium, Curr. Appl. Phys. 19 (2018) 37–43.
[32] Divya Singh, Avinash parashar, Effect of symmetric and asymmetric tilt grain boundaries on the tensile behaviour of bcc-Niobium, Comput. Mater. Sci. 143 (2018) 126–132.
[33] Avinash Parashar, Divya Singh, Molecular Dynamics based study of an irradiated single crystal of niobium, Comput. Mater. Sci. 131 (2017) 48–54.
[34] Divya Singh, Avinash Parashar, Atomistic simulations to study the effect of Nb precipitate on fracture properties of bi-crystalline Zr, J. Phys. D Appl. Phys. 52 (2019), 355304 (published online), https://doi.org/10.1088/1361-6463/ab1e34.

[35] Divya Singh, Avinash Parashar, Effect of Nb precipitate on defect formation and migration energies in bi-crystalline Zr, Mater. Chem. Phys. 235 (2019), 121729 (published online), https://doi.org/10.1016/j.matchemphys.2019.121729.
[36] Yuchen Wang, Jihong Li, Hengqiang Ye, Structure analysis of the σ equals; 7 ((1230)/[0001] 21.8°) grain boundary in α-Ti, Philos. Mag. A 73 (1996) 213–222.
[37] M. Zhou, A new look at the atomic level virial stress: on continuum-molecular system equivalence, Proc. R. Soc. A 459 (2003) 2037.
[38] Baocheng Yang, Shuaiwei Wang, Yanzhen Guo, Jinyun Yuan, Yubing Si, Shouren Zhang, Houyang Chen, Strength and failure behavior of a graphene sheet containing bi-grain-boundaries, RSC Adv. 4 (2014) 54677–54683.
[39] Shuaiwei Wang, Baocheng Yang, Shouren Zhang, Jinyun Yuan, Yubing Si, Houyang Chen, Mechanical properties and failure mechanisms of graphene under a central load, ChemPhysChem 15 (2014) 2749–2755.
[40] Shuaiwei Wang, Yubing Si, Jinyun Yuan, Baocheng Yang, Houyang Chen, Tunable thermal transport and mechanical properties of graphyne heterojunctions, Phys. Chem. Chem. Phys. 18 (2016) 24210–24218.
[41] Shuaiwei Wang, Zhaochuan Fan, Yan Cui, Shouren Zhang, Baocheng Yang, Houyang Chen, Fracture behaviors of brittle and ductile 2D carbon structures under uniaxial tensile stress, Carbon 111 (2017) 486–492.
[42] Daniel Faken, Hannes Jónsson, Systematic analysis of local atomic structure combined with 3D computer graphics, Comput. Mater. Sci. 2 (1994) 279–286.
[43] Stukowski Alexander, Structure identification methods for atomistic simulations of crystalline materials, Model. Simul. Mater. Sci. Eng. 20 (2012), 045021.